Typeset with jjap2.cls <ver.1.0> **Regular Paper**

Elastic-Constant Measurement in Oxide and Semiconductor Thin Films by Brillouin Oscillations Excited by Picosecond Ultrasound

Hirotsugu OGI, Tomohiro SHAGAWA, Nobutomo NAKAMURA, Masahiko HIRAO, Hidefumi ODAKA[1], and Naoto KIHARA[1]

Graduate School of Engineering Science, Osaka University, 1-3 Machikaneyama, Toyonaka, Osaka 560-8531, Japan

[1] *Research Center, Asahi Glass Co., Ltd., Yokohama, 221-8755, Japan*

In this study, an elastic-stiffness evaluation in transparent or translucent thin films using Brillouin oscillations detected by picosecond ultrasound is conducted. An ultrahigh-frequency (>∼50 GHz) strain pulse is generated using femtosecond light pulse in specimens and observed to propagate in the film-thickness direction. The time-delayed probe light pulse enters the specimen, which is diffracted by a strain pulse, causing oscillations in the reflectivity change of the probe light pulse. The oscillation frequency gives the elastic modulus with ellipsometry for refractive index. The theoretical calculation predicts the accuracy of stiffness measurement. The methodology is applied to the study of amorphous silica, amorphous tantalum oxide, diamond thin films, and silicon wafers.

1. Introduction

Extensive studies of the elastic properties of oxide and semiconductor materials appear[1–4] because of their important applications in high-frequency resonators.[5–8] These materials are systematically fabricated by film deposition techniques in devices and their elastic constants are definitely required. The elastic constants inherently reflect the strength for bond bending and bond stretching between atoms. Furthermore, they are sensitive to zero-volume defects such as micro- to nano-cracks,[9–11] noncohesive bonds between grains,[12–14] and soft precipitates.[15] Thus, measuring the elastic constants allows a nondestructive evaluation of thin films and they can be an absolute measure of reliability.

We here propose a noncontacting elastic-constant measurement of transparent and translucent thin films using Brillouin oscillations based on picosecond laser ultrasound. Thomsen *et al.*[16,17] have succeeded in observing high-frequency (∼50 GHz) coherent acoustic phonons in thin films using ultrafast pump-probe light pulses. Their work has been followed by several works, establishing the picosecond ultrasound technique, which involves three methods. The first is the pulse-echo method,[13,17–19] where the acoustic pulse generated by the pump light repeats reflections between the film surface and the film-substrate interface. Round-trip time and echo amplitudes are measured to determine sound velocity and attenuation. The second is phonon-resonance spectroscopy,[19–21] where we detect standing waves in nanostructures to

evaluate the elastic constants through their resonance frequencies. The third is the Brillouin oscillation,[17,22–25] which arises from interference between the light reflected at the specimen and the light refracted by the acoustic wave propagating in a transparent or translucent material.

Here, we establish the elastic-constant determination using Brillouin oscillations, theoretically confirm its reliability, and study the sensitivity of the stiffness to thin defects. The materials are amorphous silica (a-SiO_2), amorphous tantalum oxide (a-Ta_2O_5), chemical-vapor-deposited (CVD) diamond thin films, and silicon wafer.

2. Experimental Procedure

We deposited a-SiO_2 thin films and a-Ta_2O_5 thin films on a (001) Si substrate by the DC-sputtering method, using Si and Ta as sputtering targets, respectively. Also, we deposited a diamond thin film on a SiC substrate by hot-filament CVD.

We measured the refractive index n of the specimens by the ellipsometry of thin films:[26] The ellipsometric angle Ψ was measured as a function of the wavelength between 380 and 1700 nm, and the Lorentz-oscillation model was fitted to extract parameters required for calculating refractive index. Three independent measurements were conducted for three incident angles of 60, 70, and 75° for each specimen, and the results were used together in the fitting calculation.

Before the acoustic measurements, we deposited 10-nm-thick aluminum thin films on the specimens to generate the strain pulse through the thermal expansion of the aluminum layer induced by the pump pulse. Figure 1 shows the optics. A mode-locking titanium-sapphire pulse laser launches a light pulse of 800 nm wavelength with a 100 fs pulse width and a 80 MHz repetition frequency. They are split into the pump and probe pulses by the polarization beam splitter (PBS). The former (pump light) is reflected by the corner reflector and is subjected to an amplitude modulation of 100 kHz induced by an acoustic-optic crystal, and then is focused on the specimen surface to generate a strain pulse. The latter (probe light) is frequency-doubled and focused on the specimen surface perpendicularly. Parts of the probe light and reflected probe light enter the photodetectors, and their difference is fed to a lock-in amplifier to detect the amplitude and phase at the modulation frequency. By changing the light path of the pump light, we can detect the time-resolved reflectivity change, involving Brillouin oscillations.

3. Results

Figure 2 shows the reflectivity changes observed in the a-SiO_2 and a-Ta_2O_5 thin films as well as in diamond thin films. In the a-SiO_2/Si specimen, the low-frequency Brillouin oscillation appears first and then decaying high-frequency Brillouin oscillation occurs. They are from the a-SiO_2 film and Si substrate, respectively, as will be shown later. Single-frequency components appear in the a-Ta_2O_5 and diamond thin films because of their much larger thick-

nesses (see Table I). Figure 3 shows the corresponding Fourier spectra, indicating Brillouin oscillation frequencies.

Figure 4 shows the typical result for the ellipsometry refractive-index measurement. The ellipsometric angle Ψ predicted by the Lorentz-oscillation model agrees well with the measurement, providing a reliable refractive index as a function of wavelength. We used 400 nm probe light, and a refractive index of 400 nm to determine stiffness.

4. Discussion

The Bragg condition has been assumed for relating the Brillouin oscillation frequency f_{BO} with the sound velocity v and the wavelength of the probe light λ. It takes the form

$$f_{BO} = \frac{2nv}{\lambda}, \tag{1}$$

in the case of the normal incidence of probe light. Equation (1) indicates that we can determine sound velocity and then elastic stiffness by measuring Brillouin-oscillation frequency. However, this equation originates from the first-order approximation for strain, and we have to investigate its applicability to the stiffness determination by calculating the reflectivity change, considering the multiple reflections of the light pulse in the presence of the acoustic strain. Also, fewer oscillations appear in thinner films, deteriorating the accuracy of the frequency determination via Fourier transformation. We therefore reconstruct the Brillouin oscillation by assuming the elastic constant of the thin film, and validate the applicability of eq. (1) by comparing the predicted elastic constant with the input value (correct value). First, we assume the elastic constant of a thin film. Second, we simulate the reflectivity change ΔR as described below. Third, we extract the Brillouin oscillation from the film layer in the ΔR response and determine Brillouin-oscillation frequency by performing Fourier transformation with the hanning window. Finally, we deduce the longitudinal-wave elastic constant C_L from Eq. (1) and compare it with the assumed value.

Recently, we formulated the reflectivity change of the probe light pulse in a film/substrate specimen, following Thomsen et al.,[17] and analyzed the time-resolved reflectivity change caused by the strain pulse propagation. We included the frequency-dependent attenuation effect in the strain pulse by lowering the amplitude of the Fourier components using the frequency dependence of attenuation. Then, the inverse Fourier transform was used to reconstruct the strain distribution.[25] The change in the reflection coefficient r caused by the strain pulse can be written as $r = r_0 + \Delta r_f + \Delta r_s$, where Δr_f and Δr_s are the reflectivity changes caused in the film and substrate, respectively. (r_0 denotes the reflectivity without the strain pulse.) Thus, the reflectivity change is given by $\Delta R = |r_0 + \Delta r_1 + \Delta r_2|^2 - |r_0|^2$. Figure 5 shows a comparison of the measured and calculated reflectivity changes for an a-SiO_2 thin film deposited on (001) Si. The calculation shows excellent agreement with the measurement, confirming the theoretical model. Then, it is compared with the input value (accurate value)

to see their agreement.

Figure 6 shows the typical result, compared with the input elastic constant and the one deduced using eq. (1). The horizontal axis is the film thickness normalized by the wavelength of the acoustic wave, λ_{AC}, in the film. The error of the elastic constant determined using eq. (1) is estimated to be smaller than 1% when the film thickness is three times larger than the wavelength. However, the stiffness cannot be accurately evaluated for thin films with a thickness comparable to the wavelength. It is possible to determine the elastic constant from high-frequency pulse-echo signals even when the film thickness is smaller than λ_{AC}. In this case, however, film thickness must be accurately known, which is a difficult task. The Brillouin-oscillation method thus has the advantage that it does not require film thickness for determining elastic stiffness.

Table I shows comparison of the longitudinal-wave moduli C_L of the oxide thin films and Si substrate determined using eq. (1) with the reported values. The Brillouin-oscillation frequency of Si is very high because of the high refractive index of Si at 400 nm. The determined elastic modulus agrees with the reported C_{11} of monocrystal Si by 0.2% error. Thus, the elastic-stiffness determination using Brillouin oscillation is well applicable.

We measure the elastic constant of two a-SiO_2 thin films, namely, a-SiO_2 films 1 and 2, deposited at different sputtering rates (0.8 and 4.4 Å/s, respectively). a-SiO_2 film 1 shows a higher modulus and a-SiO_2 film 2 shows a lower modulus than the bulk values. Their microstructures are observed by field-emission scanning microscopy (not shown). a-SiO_2 film 1 shows a very smooth microstructure and we fail to observe any defects. The microstructure of a-SiO_2 film 2 is almost identical to that of film 1, but it appears to contain granular structures. However, there are no visible volume defects, showing a dense microstructure, despite the fact that the stiffness is lower than the other film by 10%. The increased modulus in an a-SiO_2 film was discussed in the previous study[25] and it is attributed to the reduction in the number of the membered ring of the tetrahedral SiO_4 unit. The softened stiffness can be caused by thin defects even with a very low volume fraction. We made micromechanics calculation[12,30,31] to investigate this influence. The result is shown in Fig. 7, demonstrating that defects with a high aspect ratio can decrease stiffness markedly. Defects of 1000 aspect ratio, for example, decrease the stiffness by 20% with a volume fraction of 0.1%. This result indicates that the stiffness measurement is useful for the nondestructive evaluation of thin films, because thin defects or incohesive bonds easily appear at boundaries between grains and granular structures in thin films.

We show the longitudinal-wave modulus in the tantalum oxide film in Table I. The reported value[29] is significantly smaller than our value. However, considering the sharp Fourier spectrum in Fig. 3 originating from many oscillation cycles, we think that our value seems more reliable.

Table I also shows the elastic constant of the CVD diamond film compared with the bulk value, which is calculated by the direction-over-averaging method (Hill averaging) assuming an isotropic polycrystalline material. The measured modulus is larger than the bulk value by 0.9%, which will be caused by texture: We perform an X-ray diffraction measurement, which indicates that the [111] direction of grains predominantly (but not so significantly) aligns in the film thickness direction, increasing longitudinal-wave velocity along this direction. Assuming the complete [111] texture, we obtain C_L to be 1197 GPa, which is higher than the measured value by 4%.

5. Conclusions

We presented an elastic-constant measurement method using Brillouin oscillations excited and detected by picosecond ultrasound. The numerical simulation demonstrated that the elastic stiffness can be determined by an error less than 1% when the film thickness is three times larger than the wavelength of the acoustic wave or more. This method is applied to the Si substrate, amorphous thin films, and a CVD diamond film. The determined modulus showed a favorable agreement with the reported values except for tantalum oxide.

References

1) J. Kushibiki, I. Takanaga, and S. Nishiyama: IEEE Trans. Ultrason. Ferroelectr. Freq. Control **49** (2002) 125.

2) H. Ogi, M. Fukunaga, M. Hirao, and H. Ledbetter: Phys. Rev. B **69** (2004) 024104.

3) H. Ogi, T. Ohmori, N. Nakamura, and M. Hirao: J. Appl. Phys. **100** (2006) 053511.

4) M. Arakawa, J. Kushibiki, Y. Ohashi and K. Suzuki: Jpn. J. Appl. Phys. **45** (2006) 4511.

5) S. Rabaste, J. Bellessa, A. Brioudea, C. Bovier, J. C. Plenet, R. Breniera, O. Marty, J. Mugnier, and J. Dumas: Thin Solid Films **416** (2002), 242.

6) S. Rey-Mermet, R. Lanz, and P. Muralt: Sens. Actua. B **114** (2006), 681.

7) M. Ueda, M. Hara, S. Taniguchi, T. Yokoyama, T. Nishihara, K. Hashimoto, and Y. Satoh: Jpn. J. Appl. Phys. **47** (2008) 4007.

8) H. Nakamura, H. Nakanishi, T. Tsurunari, K. Matsunami, Y. Iwasaki, K. Hashimoto, and M. Yamaguchi: Jpn. J. Appl. Phys. **47** (2008) 4052.

9) H. Ogi, G. Shimoike, M. Hirao, K. Takashima, and Y. Higo: J. Appl. Phys. **91** (2002) 4857.

10) N. Nakamura, H. Ogi, and M. Hirao: Acta Mater. **52** (2004) 765.

11) N. Nakamura, H. Ogi, T. Shagawa, and M. Hirao: Appl. Phys. Lett. **92** (2008) 141901.

12) H. Ogi, N. Nakamura, H. Tanei, R. Ikeda, M. Hirao, and Mikio Takemoto: Appl. Phys. Lett. **86** (2005) 231904.

13) N. Nakamura, H. Ogi, T. Yasui, M. Fujii, and M. Hirao: Phys. Rev. Lett. **99** (2007) 035502.

14) H. Tanei, N. Nakamura, H. Ogi, M. Hirao, R. Ikeda: Phys. Rev. Lett. **100** (2008) 016804.

15) R. Tarumi, N. Hayama, M. Hirao, Y. Higo, H. Kimura, and A. Inoue: Jpn. J. Appl. Phys. **47** (2008) 3807.

16) C. Thomsen, J. Strait, Z. Vardeny, H. J. Maris, J. Tauc, and J. J. Hauser: Phys. Rev. Lett. **53** (1984) 989.

17) C. Thomsen, H. T. Grahn, H. J. Maris, and J. Tauc: Phys. Rev. B **34** (1986) 4129.

18) O. B. Wright, B. Perrin, O. Matsuda, and V. E. Gusev: Phys. Rev. B **64** (2001) 081202.

19) H. Ogi, M. Fujii, N. Nakamura, T. Yasui, and M. Hirao: Phys. Rev. Lett. **98** (2007) 195503.

20) H. Ogi, M. Fujii, N. Nakamura, T. Shagawa, and M. Hirao: Appl. Phys. Lett. **90** (2007) 191906.

21) N. Nakamura, H. Ogi, and M. Hirao: Phys. Rev. B **77** (2008) 245416.

22) A. Devos and R. Côte: Phys. Rev. B **70** (2004) 125208.

23) A. Devos, M. Foret, S. Ayrinhac, P. Emery, and B. Rufflé: Phys. Rev. B **77** (2008) 100201.

24) O. Matsuda, O. B. Wright, D. H. Hurley, V. E. Gusev, and K. Shimizu: Phys. Rev. Lett. **93** (2004) 095501.

25) H. Ogi, T. Shagawa, N. Nakamura, M. Hirao, H. Odaka, and N. Kihara: Phys. Rev. B **78** (2008) 134204.

26) H. G. Tompkins and W.A.McGahan: Spectroscopic Ellipsometry and Reflectometry, (Wiley, New York) 1999.

27) H. Ledbetter and S. Kim: Monocrystal elastic constants and derived properties of the cubic and the hexagonal elements: in Handbook of Elastic Properties of Solids, Liquids, and Gases, (Academic, San Diego), Vol. 2, 2001.

28) D. Fraser: J. Appl. Phys. **39** (1968) 5868.

29) H. Hirakata, S. Matsumoto, M. Takemura, M. Suzuki, and T. Kitamura: Int. J. Soli. Struc. **44** (2007) 4030.

30) T. Mura: Micromechanics of Defects in Solids, (Martinus Nijhoff, Dordrecht), 2nd ed., 1987.

31) T. Mori and K. Tanaka: Acta Metall. **21** (1973) 571.

Table I. Brillouin-oscillation frequencies f_{BO}, refractive indexes n, film thicknesses d, longitudinal-wave velocities v_L, and Longitudinal-wave moduli C_L of oxides and semiconductors determined in this study.

	f_{BO} (GHz)	n	d (nm)	v_L (m/s)	C_L (GPa)
Si substrate	235.2	5.57	-	8445	166.1
Reported (bulk)[27]	-	-	-	8437	165.8
a-SiO_2 film 1	45.89	1.479	569.4	6201	84.6
a-SiO_2 film 2	42.74	1.444	1239	5936	77.5
Reported (bulk)[28]	-	-	-	5935-5993	77.5-79.2
a-Ta_2O_5	51.37	2.32	4718	4428	171.2
Reported (film)[29]	-	-	-	-	139
CVD diamond film	223.7	2.47	50000	18113	1153
Reported (bulk)[27]	-	-	-	18030	1143

Figure Captions

Fig. 1 Optics for the pump-probe measurement for observing Brillouin oscillations.

Fig. 2 Brillouin oscillations observed in a-SiO_2 film (569 nm) on (001) Si substrate, a-Ta_2O_5 film (4718 nm) on (001) Si substrate, and CVD diamond film (50000 nm) on SiC substrate. The slowly decreasing backgrounds have been removed using low-order polynomial functions.

Fig. 3 Fourier spectra of Brillouin oscillations in Fig. 2.

Fig. 4 (Color on line) Wavelength dependence of measured (black lines) and calculated (red lines) ellipsometry angles at three incident angles for an a-SiO_2 film.

Fig. 5 (Color on line) Measured (black lines) and calculated (red lines) reflectivity changes for a-SiO_2 film (300 nm) on (001) Si substrate.

Fig. 6 Estimated error in the elastic constant determined using eq. (1) for various thickness/acoustic-wavelength ratios.

Fig. 7 Modulus decrease caused by thin pancake-shaped air inclusions with various aspect ratios calculated by micromechanics modeling. The numbers indicate the aspect ratio. First, the hexagonal-symmetry elastic constants with oriented inclusions are calculated using the Mori-Tanaka mean-field theory,[31)] and then the direction-over-averaging elastic constants are calculated using the Hill-averaging method.

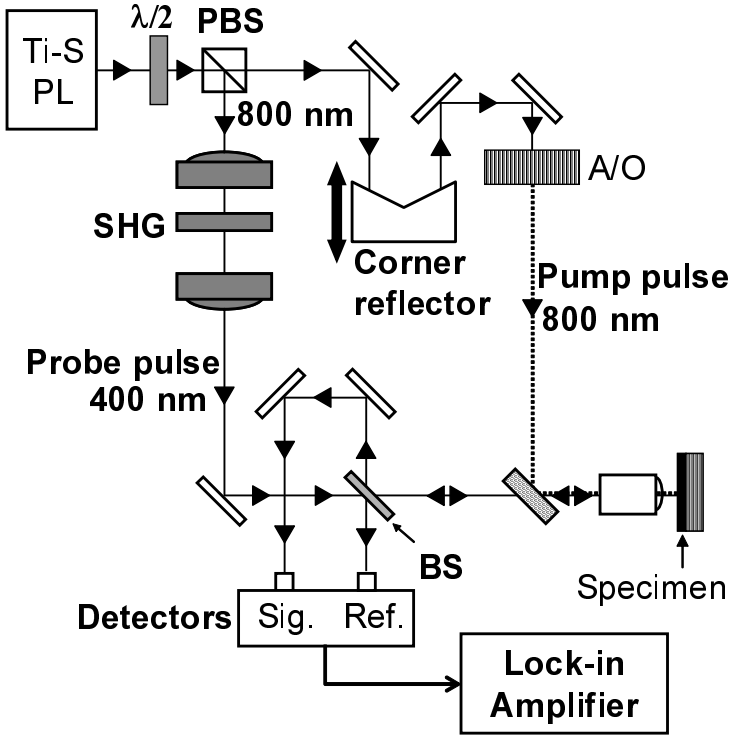
Ti-S
PL
λ/2
PBS
800 nm
A/O
SHG
Corner
reflector
Pump pulse
800 nm
Probe pulse
400 nm
BS
Specimen
Detectors
Sig.
Ref.
Lock-in
Amplifier

Fig. 1.

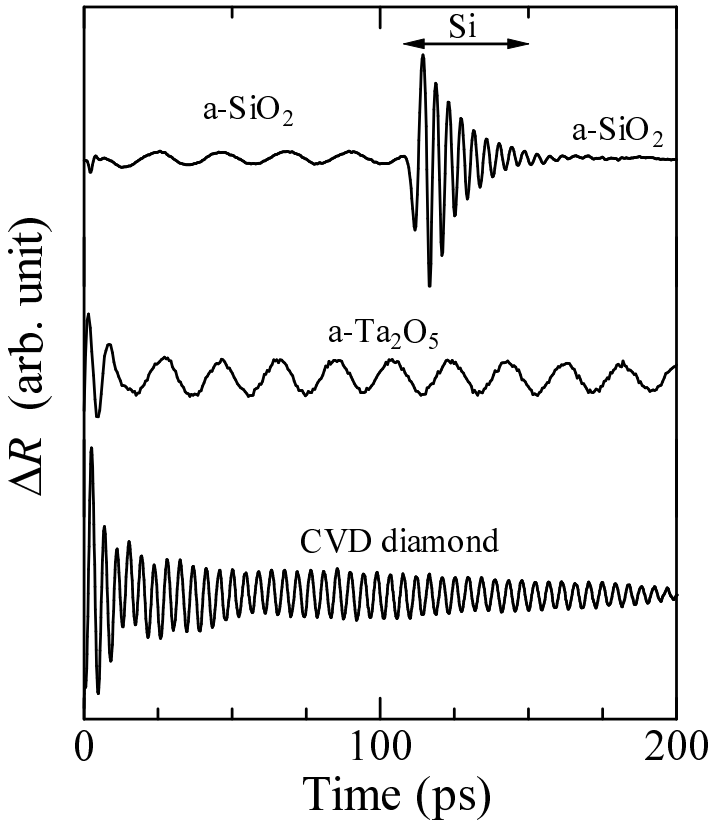
Si
a-SiO2
a-SiO2
a-Ta2O5
CVD diamond
ΔR (arb. unit)
0
100
200
Time (ps)

Fig. 2.

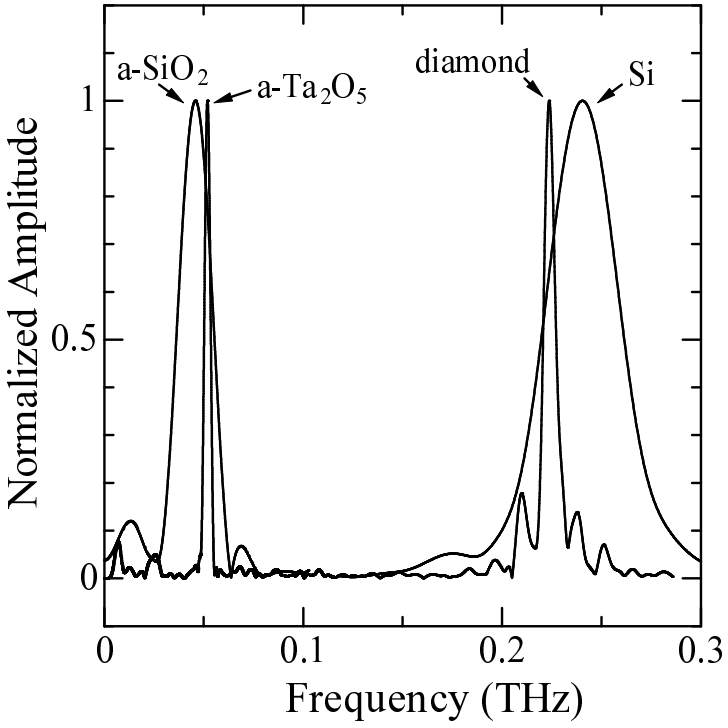
a-SiO2
a-Ta2O5
diamond
Si
Normalized Amplitude
1
0.5
0
0
0.1
0.2
0.3
Frequency (THz)

Fig. 3.

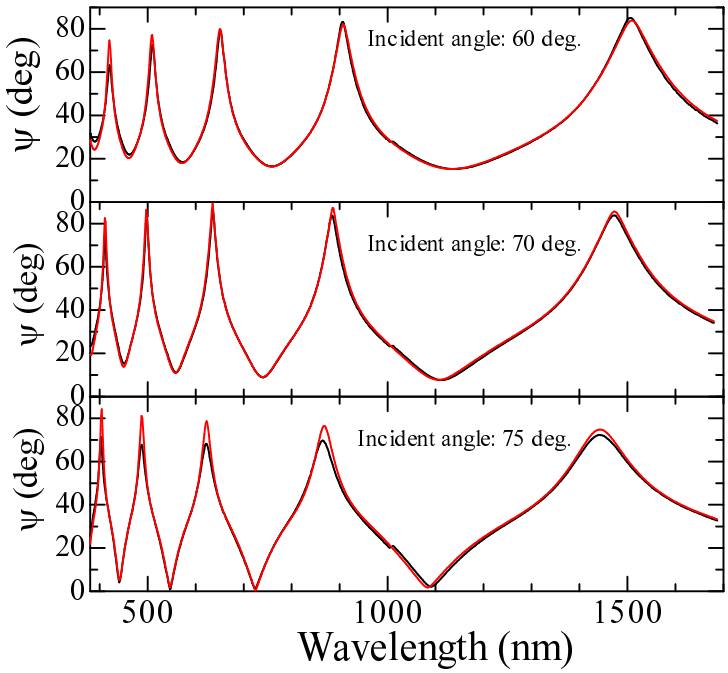
Incident angle: 60 deg.
Incident angle: 70 deg.
Incident angle: 75 deg.
ψ (deg)
0
20
40
60
80
500
1000
1500
Wavelength (nm)

Fig. 4.

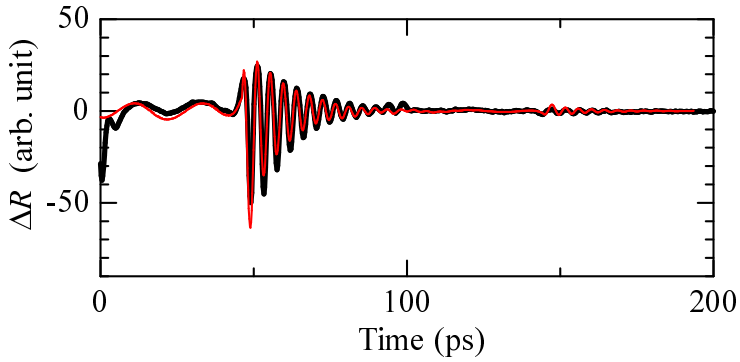

Fig. 5.

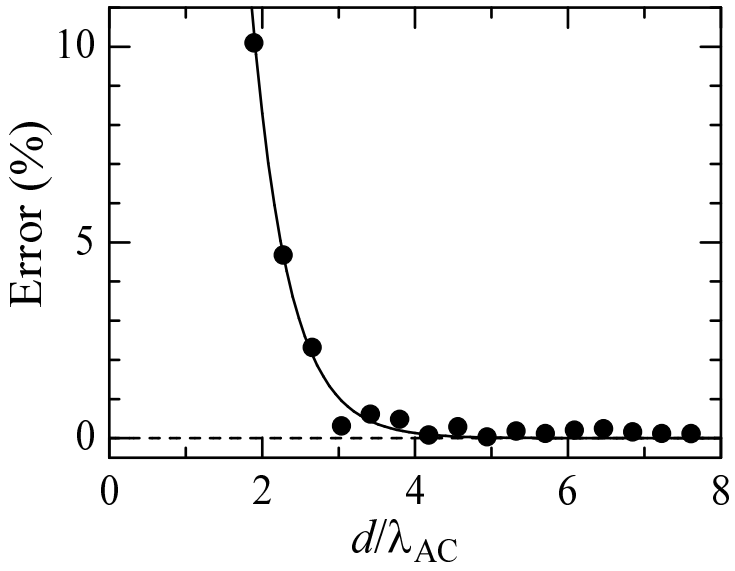

Fig. 6.

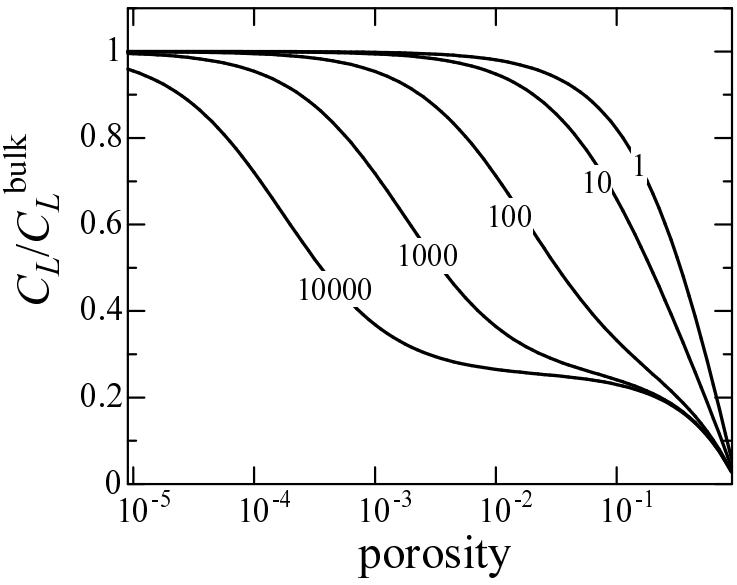
1
0.8
0.6
0.4
0.2
0
C_L/C_L^{bulk}
10^{-5}
10^{-4}
10^{-3}
10^{-2}
10^{-1}
porosity
1
10
100
1000
10000

Fig. 7.